Wiley
International Journal of RF and Microwave Computer-Aided Engineering
Volume 2024, Article ID 6490949, 18 pages
https://doi.org/10.1155/mmce/6490949

WILEY

Research Article

A Wearable Dual-Band Dual-Polarized Patch Antenna for ISM Range Applications

Pouria Shams and Mohammad Amin Honarvar

Department of Electrical Engineering, Najafabad Branch, Islamic Azad University, Najafabad, Iran

Correspondence should be addressed to Mohammad Amin Honarvar; amin.honarvar@gmail.com

Received 15 February 2024; Revised 4 October 2024; Accepted 7 November 2024

Academic Editor: Trushit Upadhyaya

A compact low-profile dual-band dual-polarized wearable patch antenna, capable of working in 2.4 and 5.8 GHz ISM band for either on-body or off-body applications with different radiation patterns in each working band, is presented in this paper. The fabricated antenna consists of four layers including modified ground and patch layers and two dielectric layers made of jean fabric, and it has a radius of 30 mm with overall height of 3.4 mm fed by a single probe. The proposed structure is designed in a way that is capable of radiating linearly polarized (LP) waves in lower working frequency and circularly polarized (CP) waves in its upper working band. The ground plane is modified to ensure the dual-band radiation as well as miniaturization of the antenna. The patch of the antenna benefits from truncated corners and four circular stubs which are practically coupled with antenna's modified ground to provide desired axial ratio and dual polarization capability. With the help of computer-based simulations, the antenna is placed on human body tissue and the calculated amount of SAR values in each band for 1 g tissue is 0.15 and 0.89 Wkg, respectively, which guarantee the safety of the human body in close proximity to the antenna.

Keywords: dual band; dual polarization; ISM; SAR; wearable

1. Introduction

The compactness of radiating tools and the simplicity of fabrication and usage can be cross-reinforcing in today's medical environments. Monitoring the signals and transferring relative data with the means of miniaturized wearable structures have drawn much attention between researchers. In recent years, there has been an ongoing interest in wearable patch antennas for medical usages. Smart healthcare systems which are closely associated with wearable antennas working in wireless body area network (WBAN) are in fact obviously dependent on small-sized antennas and multiband operation as well as dual polarization capability. The fundamental role of wearable antennas in medical applications is monitoring and transferring data from other sensors like implanted capsules and related resonators to the other in-use systems for processing and gathering results. For the purpose of communicating with other on-body devices, an omnidirectional radiation pattern is highly in demand; however, to establish an efficient and reliable connection link with a device or system that is not placed on the human body, a more directional pattern is needed. The proposed antenna is designed in a way that is capable of transmitting and receiving information in 2.4 GHz ISM band with an omnidirectional radiation pattern parallel to the surface of the body, which is quite suitable for on-body communication. For the upper band which is 5.8 GHz, a fairly directional pattern is achieved. Despite having undoubted benefits of employing two different feeds with 90° of phase difference like better polarization discrimination, textile antennas seem to be more applicable using one feed indeed. While achieving polarization isolation is challenging in dual-polarized antennas due to coupling effects and proximity of input ports [1], employing novel techniques like defected ground structures (DGSs) and adding stubs to the radiator can provide designers with a dual-polarized antenna with reasonable polarization purity between channels. A lot of effort has been made to achieve all desired characteristics of a textile multiband dual-polarized antenna in previous papers. For instance, in [2], dimensions of the

antenna are quite small and ultrawideband (UWB) radiation is achieved by using coplanar waveguide feeding technique, but it does not provide circular polarization capability. In [3], the mentioned structure is only circularly polarized and suits mostly off-body communication. In [4], a reconfigurable structure with dual polarization capability is presented; however, its operation in only one band is not satisfactory. In [5], although polarization diversity is achieved through a unique balun feeding technique, the relative dimensions are not so small to be used in wearable biosensing environments. Using metamaterial unit cells or radiating elements such as CRLH radiators provides good results in miniaturization of the antenna. In [6], it is proposed as a suitable candidate for use as wearable structure, even though it is not flexible and the feeding structure is somehow intricate when used as an array. There are some brilliant studies which provide high cross-polarization discrimination (XPD), but neither is circularly polarized and wearable simultaneously [7]. Although having two different ports will provide high polarization discrimination, for wearable antennas, the simplicity of feeding network and reducing the number of ports are essential [8]. So many researches have been conducted to determine the suitable material to be used as substrate of wearable patch antennas like [8], which introduces a number of materials that omit the dependence on fixed substrate heights. There are numerous studies which demonstrate the possibility of using cotton and other thin materials as the antenna's substrate. In [9], the antenna has been printed on flexible felt substrate with relative permittivity of 1.63 and loss tangent of 0.044 that is a good choice for wearable textile patches to be printed on. In the field of body-centric communication, dual-band operation is highly in demand due to the purpose of mitigating the number of radiators in healthcare monitoring systems. There are some methods that result in multiband resonance in different frequencies, for instance, cutting slots in ground plane or main radiator [10–12].

Choosing a proper material to be used as the antenna's substrate can be quite tricky. As we go toward the material with higher permittivity, the amount of capacitance will increase; consequently, the resonance frequency decreases and rescaling the radiating elements is unavoidable. Another crucial fact that should be considered in this field of designing is the flexibility, which is fundamental in wearable devices. Using a rigid and uncomfortable surface for substrate is not a good choice for designer. As mentioned above, there should be a trade-off between the substrate permittivity and substrate height and antenna dimensions. Although high gain is not a must in wearable applications, it should be considered in a way that does not sacrifice the antenna's efficiency.

The need for a state-of-the-art wearable antenna in biosensing environments that is more user-friendly than abovementioned studies and capable of representing all the desired characteristics of a decent wearable antenna is undeniable. The purpose of this literature is to propose a low-profile dual-band dual-polarized antenna which benefits from flexible jean fabric layers as the substrate. This new design has led to exiting the antenna through one port resulting in a simplified usage possibility for the person wearing the antenna. Unlike other studies, this structure provides all the desirable characteristics like working in two different frequency bands with different polarization type in each band along with simplicity of usage and flexibility due to its substrate material. Finally, the antenna is fabricated and tested and the results are presented in the paper. This paper is organized as follows: material determination of the antenna's substrate is discussed in Section 2; results and computer-based calculations as well as the effect of the antenna on human tissue and specific absorption rate (SAR) are discussed in Section 3; antenna fabrication and measured results are demonstrated in Section 4, and concluding notes are in Section 5.

2. Material Determination and Antenna Design

There are a number of state-of-the-art researches that introduce different materials which are good candidates for dielectric layers in wearable patch antennas. In [13], wool felt and polyamide fabric are used with heights of 3.5 and 6 mm and permittivities of 1.45 and 1.14, respectively. In [14, 15], two examples of felt and cotton are used as dielectric layers, with heights of 1.1 and 2.8 mm and permittivities of 1.3 and 1.6, respectively, which seem to be suitable candidates for low-profile applications.

In [16], resonance method is employed to determine the characteristics of some flexible fabrics. Having the desired properties in mind, jean layers meet the requirements of dielectric layers in needed wearable application. In this literature, jean cotton has been used as the substrate and superstrate of the structure. Relative permittivity of the chosen fabric is 1.6, where the heights of substrate and superstrate are 2.6 and 0.7 mm, respectively.

The proposed antenna consists of four different layers. Figure 1 depicts these layers with details. Other relative dimensions are listed in Table 1. Patch and ground layers are designed with thin flexible copper with 0.038 mm thickness to ensure the bending capability of the antenna. Ground layer has been modified with four quarter circle slits near its edge and four triangular defects. The patch layer consists of a rectangle with 30 mm of length and 23 mm width laying in the *y-x* plane. The rectangular patch features two truncated corners as well as two square-type defects in other corners. The patch is mated with four bent stubs which are essential in reaching circular polarization in the upper working band. The antenna is excited through probe feeding in a symmetrical manner from the center of the ground layer. The radius of the circular antenna is 30 mm.

Defects in ground layer are designed in a way that two resonances are seen in 2.4 and 5.8 GHz, but the main advantage of the modified ground layer is reaching an omnidirectional pattern in the lower band. Radiation properties of the ground layer coupled with a truncated patch mated with long stubs are crucial in changing the antenna performance in terms of achieving circular polarization and a more directional radiation pattern in the upper working band.

The angle of patch stubs is optimized not to cover the defects in the ground layer completely. Shorter stubs

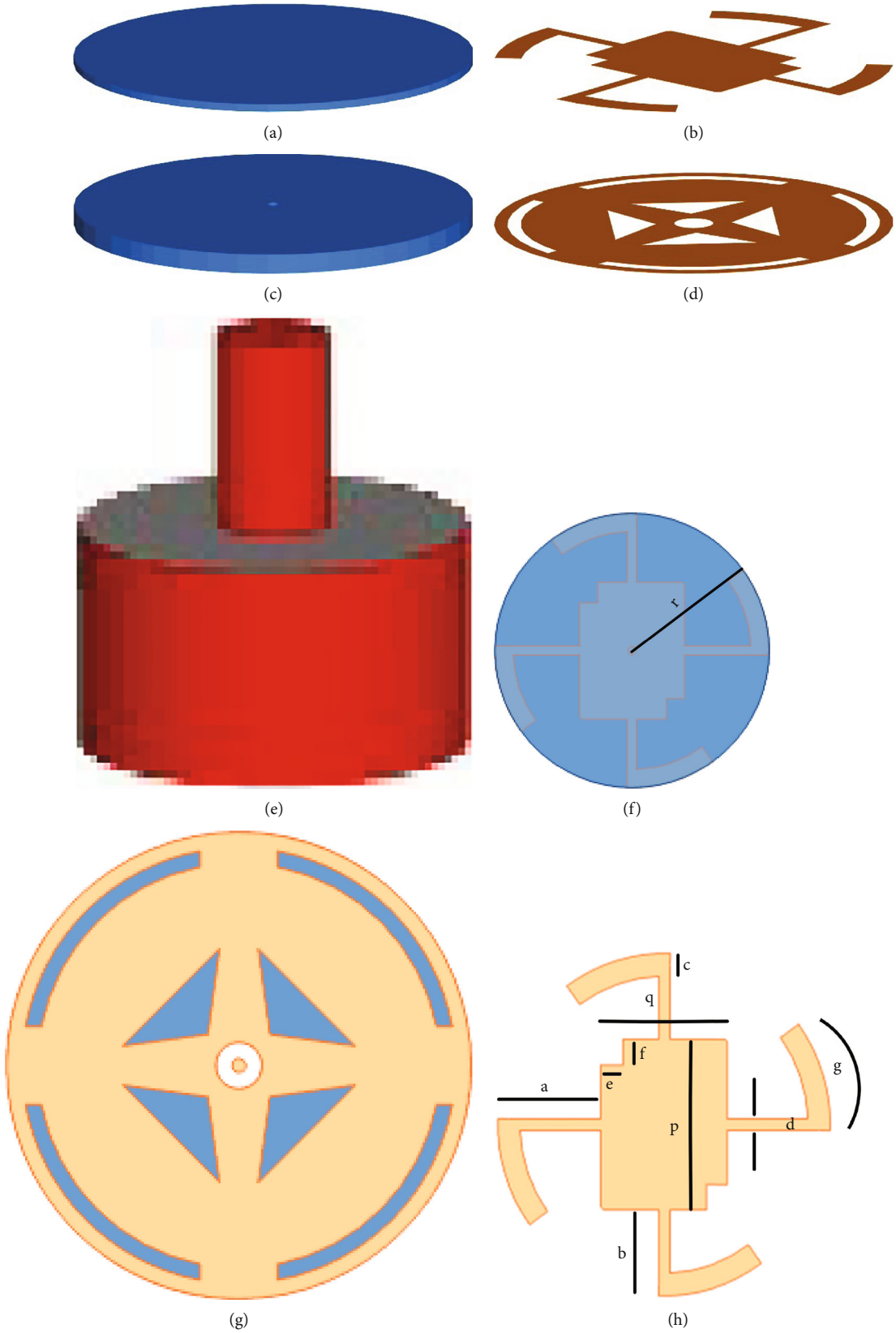

FIGURE 1: Continued.

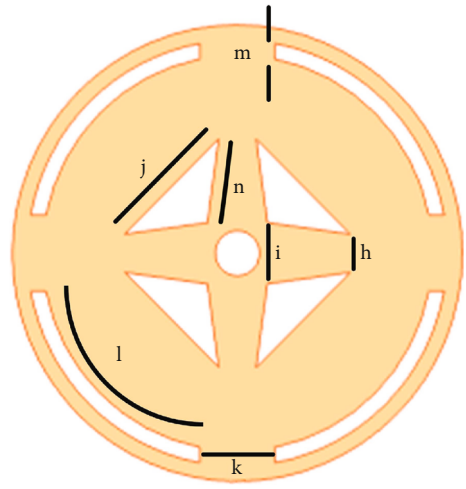

(i)

FIGURE 1: (a) Jean fabric superstrate layer with 0.7 mm height. (b) Patch layer. (c) Jean fabric substrate layer with 2.6 mm height. (d) Ground layer. (e) Probe feeding. (f) Upside view. (g) Downside view. (h) Patch dimensions. (i) Ground dimensions.

TABLE 1: Detailed dimensions of patch and ground layers.

Symbol	Value (mm)	Symbol	Value (mm)
a	18.5	*i*	8
b	15	*j*	17.6
c	4	*k*	10
d	2	*l*	34
e	4	*m*	2
f	4.5	*n*	18.4
g	15.32	*p*	30
h	5	*q*	23
r	30		

deteriorate the circular polarization properties. Nevertheless, longer ones add to the electric length of the patch. Therefore, in order not to shift the desired resonance frequencies, the length of the stubs is carefully optimized.

3. Discussion and Results

The simulations of the proposed structure are done through CST Studio Suite while measured results are done with Agilent Network Analyzer. Simulated *S* parameter is shown in Figure 2(a). Figure 2(b) demonstrates the radiation efficiency which shows the ratio of total power accepted by the antenna to the radiated power and gain of the antenna simultaneously. This wearable antenna works fairly efficient in lower and upper working bands, but due to the height of the substrate, efficiency is slightly lower than 70%. Wearable antennas are not meant to have high amount of gain values because they are mostly attached to the user's body or clothes. Accordingly, this antenna provides 3.9 dB gain in the upper working band and 1.1 dB gain in the lower working band to ensure the safety for on-body communication.

As stated above, one of the major challenges of patch antennas which provide multiband feature would be acquiring directional radiation pattern. A proportional directive pattern is reached in the proposed wearable structure with the help of defected ground layer in spite of the intrinsic antidirectional radiation pattern of the planar patches.

Mostly, circular polarized antennas use two different ports with 90° of phase difference to ensure enough polarization discrimination and enhanced circular characteristics. Couplers are widely used in structures with more than one feeding port to ensure the desired 90° of phase shift and isolation between ports. In [17], a branch-line hybrid coupler is used in feeding network of the antenna to generate circular polarization. Although this structure is fed through one feeding port, circular polarization is reached through the notable help of patch stubs mated with truncated rectangular patch, laying above the defected ground layer. Practically, antennas are considered to have circular polarization if the value of axial ratio is below 3 dB in the nominated frequency. The gathered information from different phi quantities and constant theta value over frequency sweep of the proposed structure is shown in Figure 2(c).

This antenna is left-handed circularly polarized (LHCP) in 5.8 GHz. Radiation patterns in 5.8 GHz in both *XZ* plane and *YZ* plane are presented in Figure 3.

3.1. Parametric Study of the Patch Layer. A parametric study is given in Figure 4 in order to demonstrate the effect of patch stubs and their angle on axial ratio of the antenna in the upper frequency band. It is important to consider the axial ratio values and return loss results for different stub lengths and angles in both working bands, because the longer the stubs are, the more they add to the electric length

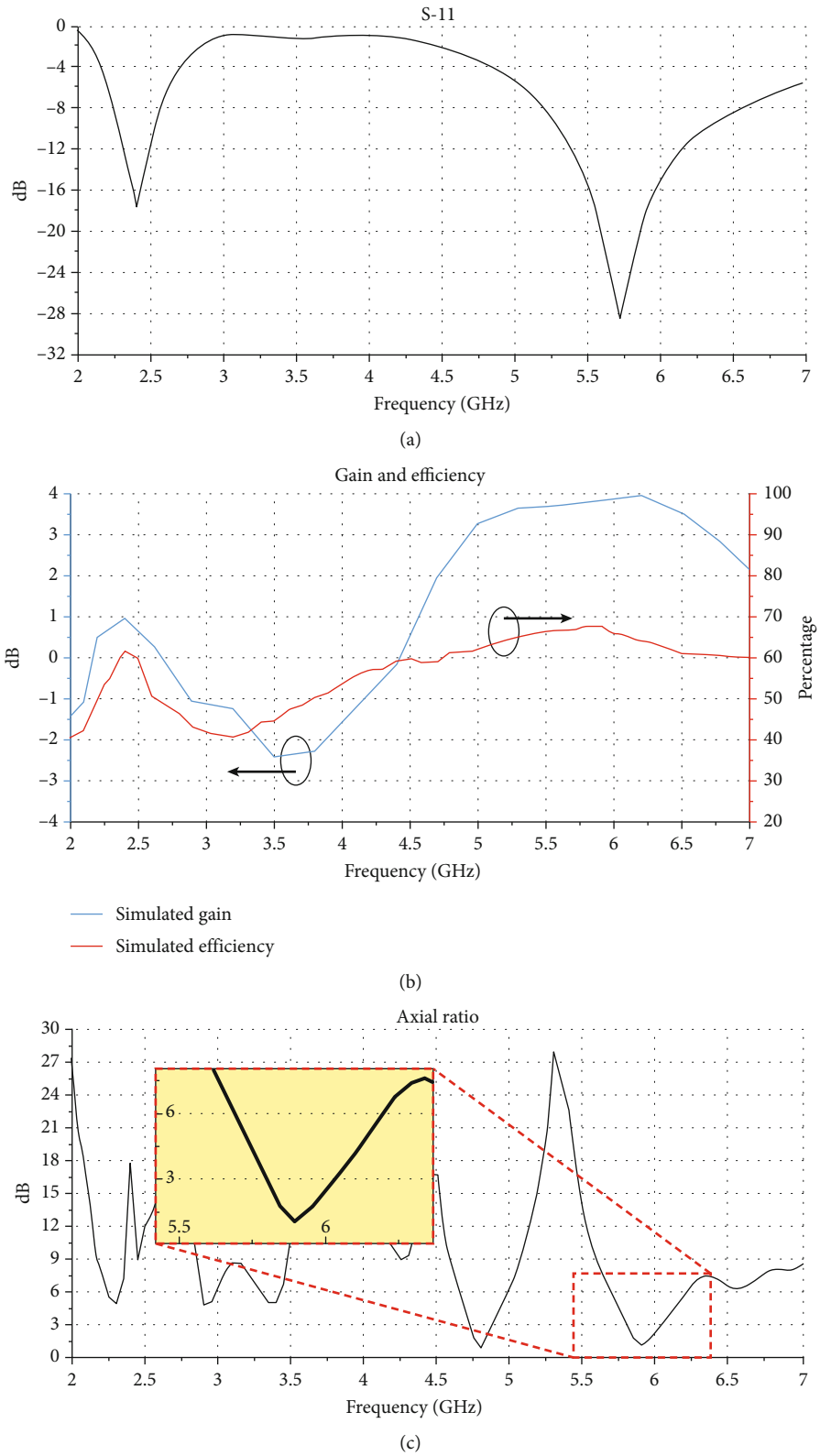

FIGURE 2: (a) Return loss in 2.4 and 5.8 GHz. (b) Simulated gain and radiation efficiency, blue line is gain and red line is efficiency. (c) Simulated axial ratio.

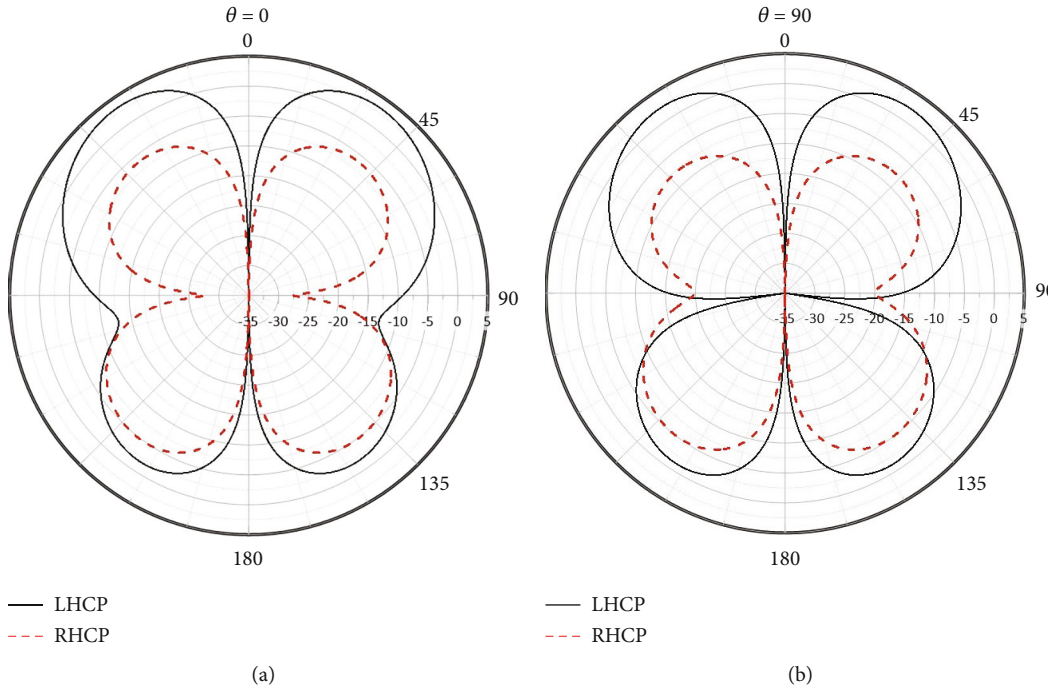

FIGURE 3: (a) LHCP and RHCP in phi = 0 in 5.8 GHz. (b) LHCP and RHCP in phi = 90 in 5.8 GHz.

of the antenna's patch and therefore it deteriorates the return loss values in the lower working band. Figure 4(a) shows the patch of the antenna without stubs. Although the value of axial ratio in 5.8 GHz is below 3 dB in this case, there is no resonance in 2.4 GHz. Figure 4(b) shows 20° patch stub angle. Obviously, there is no circular polarization in 5.8 GHz band due to axial ratio values shown in Figure 4(e) for this patch stub angle. Figure 4(c) illustrates the antenna's patch with 60° stub angle which is not desirable as well due to poor return loss result in the lower band. With the help of parametric optimization, the optimum value of 38° is found for patch stub angle (Figure 4(d)). In this configuration, the maximum axial ratio bandwidth of 2 MHz is calculated. Figures 4(e) and 4(f) show the results for return loss and axial ratio values in different stub angles and the optimum 38° stub angle.

3.2. Parametric Study of DGS. In contrast to patch layer and stubs which are responsible for resonance in the lower working band, in this antenna, DGS can play a significant role in determining the resonance frequency in the upper working band. DGS in this antenna is designed with four thin circular slots just near the edge of the ground layer and four central elements to ensure the resonance in the designated frequency. Figure 5 shows the different designs regarding DGS elements and their effects on return loss parameter and axial ratio of the antenna. Figure 5(a) illustrates the simple ground layer with four slots which can result in poor resonance in 5.8 GHz due to improper electric length of the conductor. Hence, no axial ratio is calculated and shown in Figure 5(f) for this state. Figure 5(b) shows four defected elements added to a simple ground layer without any circular slots. This would result in poor axial ratio that means no circular polarization in 5.8 GHz due to lack of coupling between patch stubs and ground layer (Figure 5(f)). Figure 5(c) shows defected ground layer with wide circular slots. Although in this case return loss value is −32 dB with 0.5 GHz bandwidth in 5.8 GHz, S parameter in the lower band is deteriorated (Figure 5(e)). On the other hand, axial ratio value is obviously enhanced with wide circular slots but the width of the slots needs to be optimized. Figure 5(d) shows the optimum width of the four circular slots which results in desirable axial ratio values.

3.3. Bending Analysis. To ensure the usability of the structure, it is important to test the antenna in different bending conditions. The antenna can be bent slightly to sit on parts like the arm or leg. Maximum bending angle to be considered is when the antenna is wrapped around the wrist of the user. These bending conditions are illustrated in Figure 6. The analysis of antenna's performance is provided in 45 and 180° bending conditions in XZ and YZ planes in Figure 7. As Figure 7(a) shows, the return loss values of the proposed antenna are still in acceptable range in both 2.4 and 5.8 GHz when bent both 45 and 180° in XZ and YZ planes with 0.5 GHz bandwidth in the upper working band and 0.2 GHz bandwidth in the lower working band. Figure 7(b) shows axial ratio parameter under mentioned bending conditions to ensure the circular polarization in 5.8 GHz. It can be derived from the figure that the values of axial ratio are under 3 dB except the situation when the antenna is bent 180° in the Y direction which is still under 5 dB. Considering 180° to be the maximum bending condition for the antenna in an actual situation, the antenna is

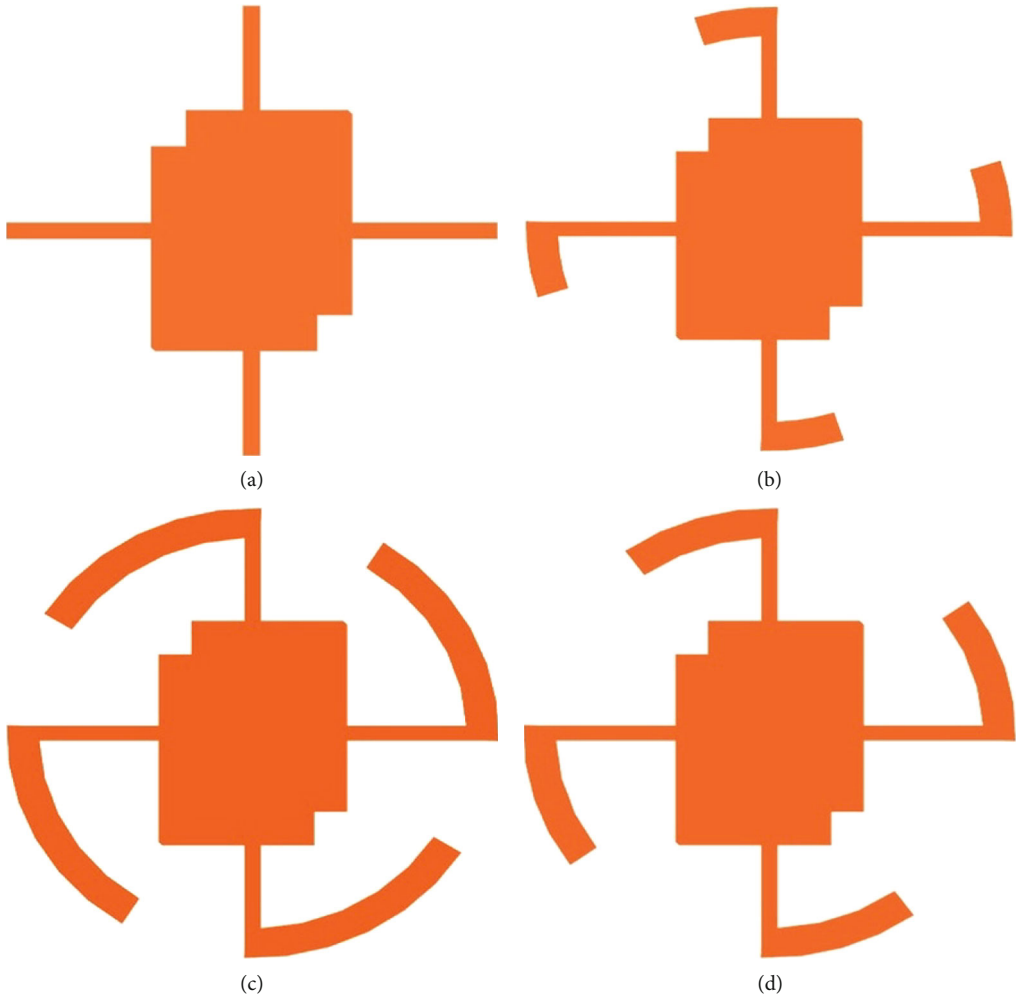

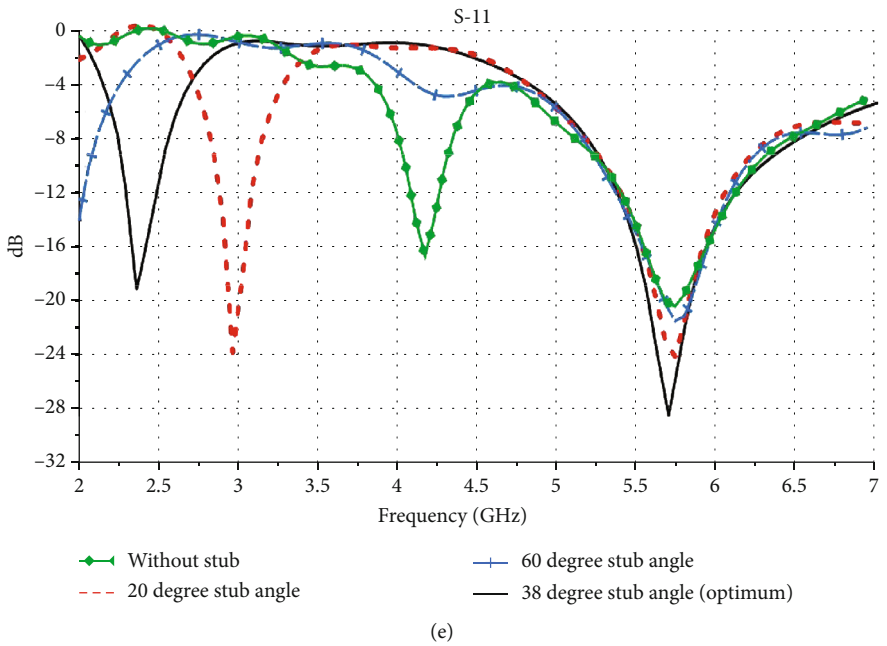

(e)

FIGURE 4: Continued.

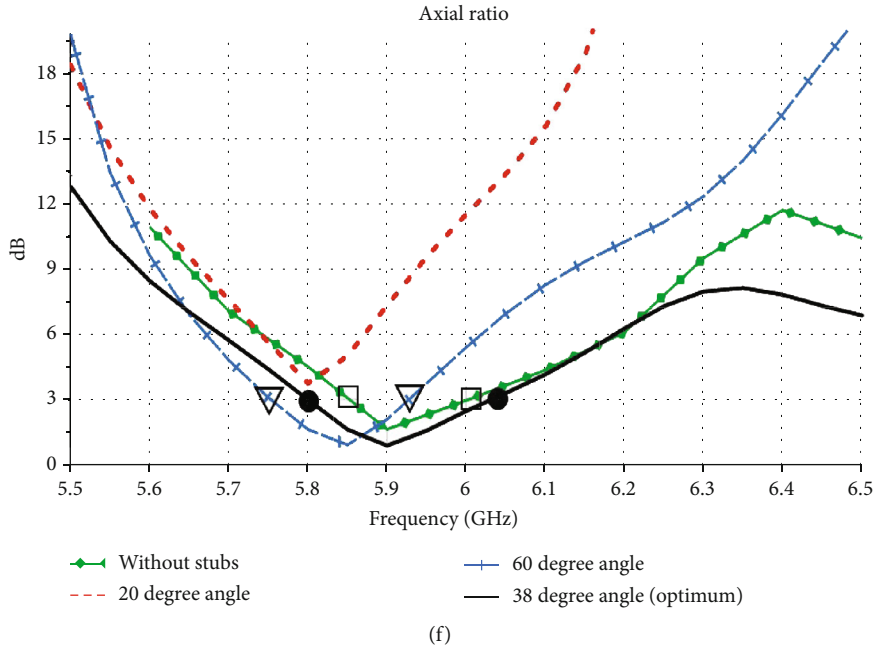

FIGURE 4: (a) Patch without stubs. (b) Twenty-degree patch stub angle. (c) Sixty-degree patch stub angle. (d) Thirty-eight–degree patch stub angle (optimum). (e) Axial ratio values in different stub angles. (f) S-11 parameter in different stub angles.

predicted to perform satisfactorily in other bending angles less than 180°.

3.4. Surface Current Analysis. In previous sections, axial ratio parameter of the proposed structure was discussed thoroughly under different circumstances to provide sufficient proof of radiation with circular polarization in 5.8 GHz. Another means to give a decent insight on circular polarization of the antenna in 5.8 GHz is to analyze the distribution of surface current in different azimuth angles in the mentioned frequency. As mentioned before, the defected ground layer is responsible for resonance in the upper working band in this structure. Hence, surface current distribution in the ground layer is illustrated in Figure 8. As Figure 8 shows, there is a clockwise patten in arrows which shows LHCP in terms of circular polarization.

3.5. On-Body Analysis and Realization Through Human Tissue Proximity and SAR. One of the major factors of wearable gadgets working in WBAN environments is not being harmful to the human body in near distances [18]. Calculating the SAR is the most known method to determine whether the antenna is capable of being used safely or not [19]. The following equations are provided to help in determination of SAR in general:

$$\mathbf{SAR} = \frac{\sigma \left| E_{\mathrm{rms},t} \right|^2}{\rho} \tag{1}$$

where σ is the conductivity of tissue (Sm) and ρ represents mass density of the material (kg(m^3)), whereas E is the electric field density (Vm). When it comes to calculating the SAR value in proximity with the human body tissue, a more functional equation is usually used as

$$\mathbf{SAR} = \frac{1}{V} \int \frac{\sigma(r) |E(r)|^2}{\rho(r)} dr. \tag{2}$$

In Equation (2), V represents the volume of the tissue sample:

$$\mathbf{SAR} = \left. \frac{c \Delta T}{\Delta t} \right|_{t=0}. \tag{3}$$

Equation (3) shows the relation between SAR and temperature in which ΔT is the temperature change (°C) and Δt is the exposure duration (s) and finally c represents the specific heat capacity (Jkg°C). Increasing the body tissue temperature is another concern integrated with the SAR calculation and acceptable SAR values [20]. Having the thermal properties of the different body layers such as skin, fat, and muscle tissues, complex simulations can be done to estimate the realized SAR values with the help of computer tools. In this literature, the CST Studio Suite has been used for complementary simulations in SAR determination. Figure 9(a) shows the antenna placed above the human body tissue. Simulated SAR values and graphic demonstrations in each frequency with the antenna placed on the human body phantom with a distance of 2 mm are presented in Figures 9(b) and 9(c). To provide a better insight, simulated S parameter and SAR analysis has been done on the antenna with different distances to the human body and results are provided in Figures 10 and 11. The electromagnetic

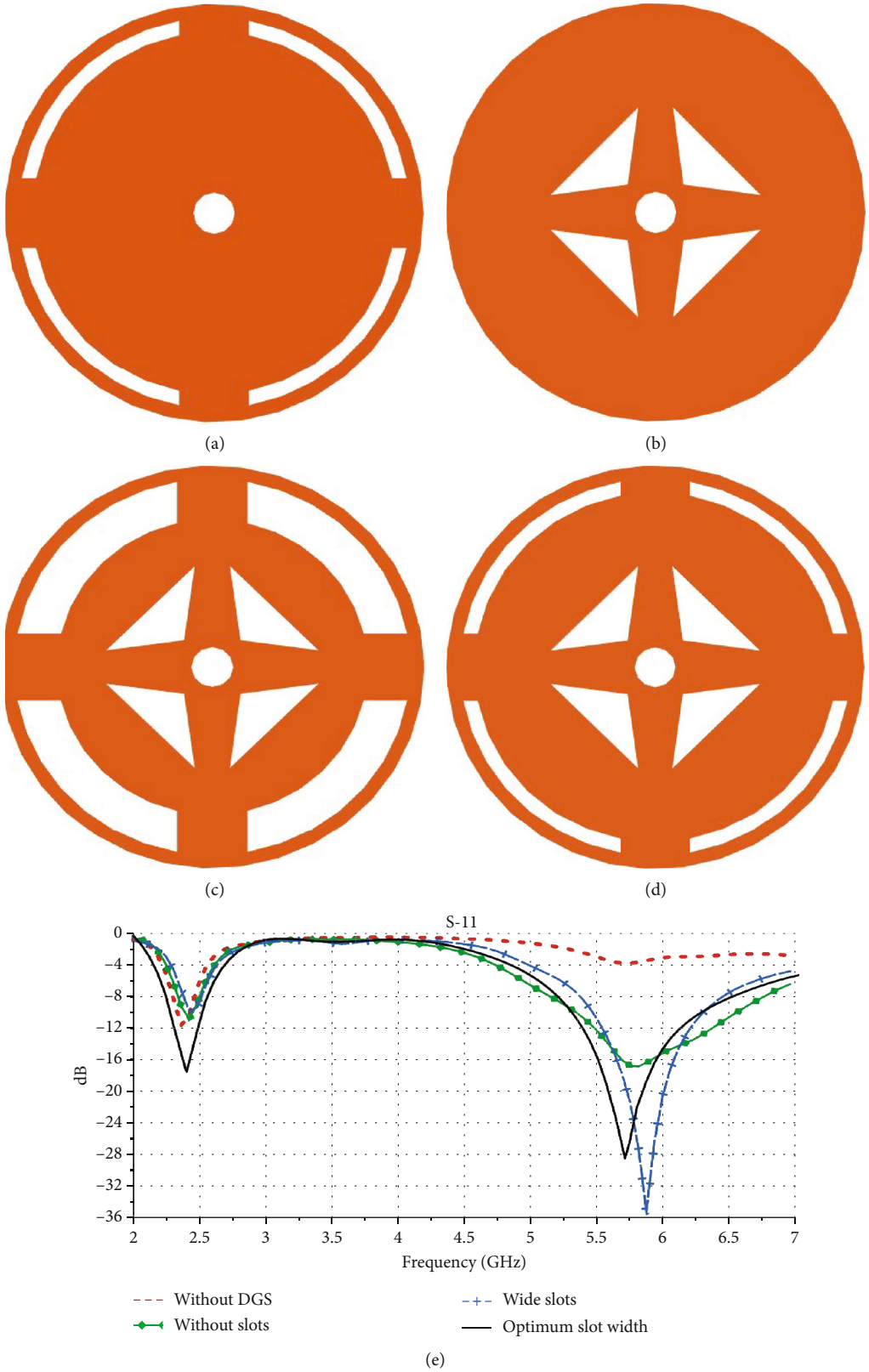

FIGURE 5: Continued.

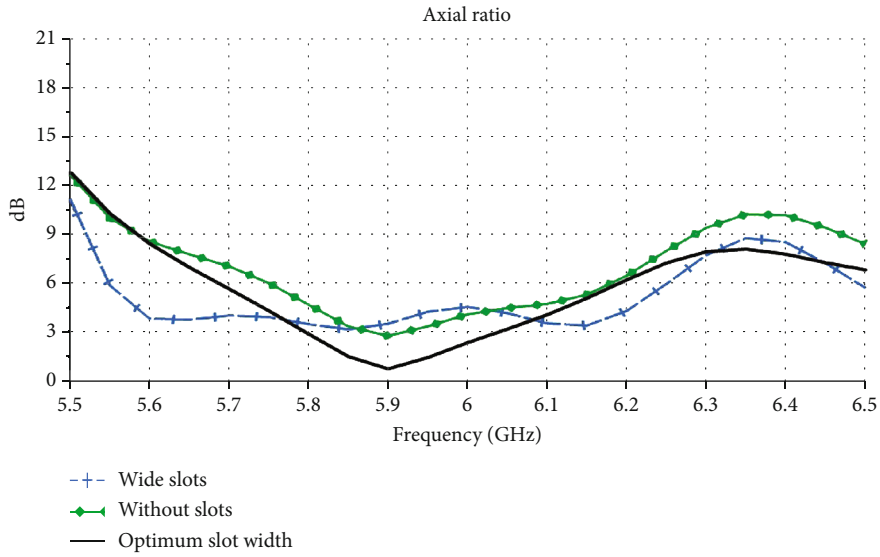

(f)

FIGURE 5: (a) Ground without DGS. (b) Ground without slots. (c) Ground with DGS and wide slots. (d) Ground with DGS and optimum slot width. (e) S-11 parameter with different ground elements. (f) Axial ratio with different ground elements.

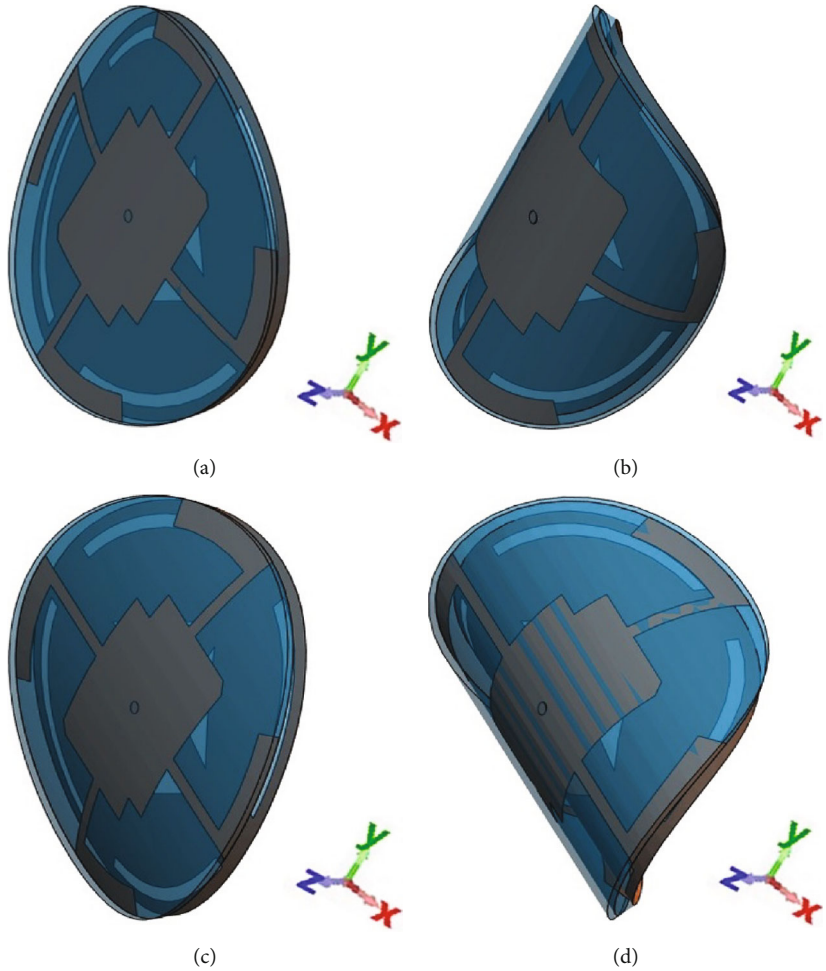

(a) (b) (c) (d)

FIGURE 6: (a) Forty-five–degree bent in the *Y* direction. (b) One hundred eighty–degree bent in the *Y* direction. (c) Forty-five–degree bent in the *X* direction. (d) One hundred eighty–degree bent in the *X* direction.

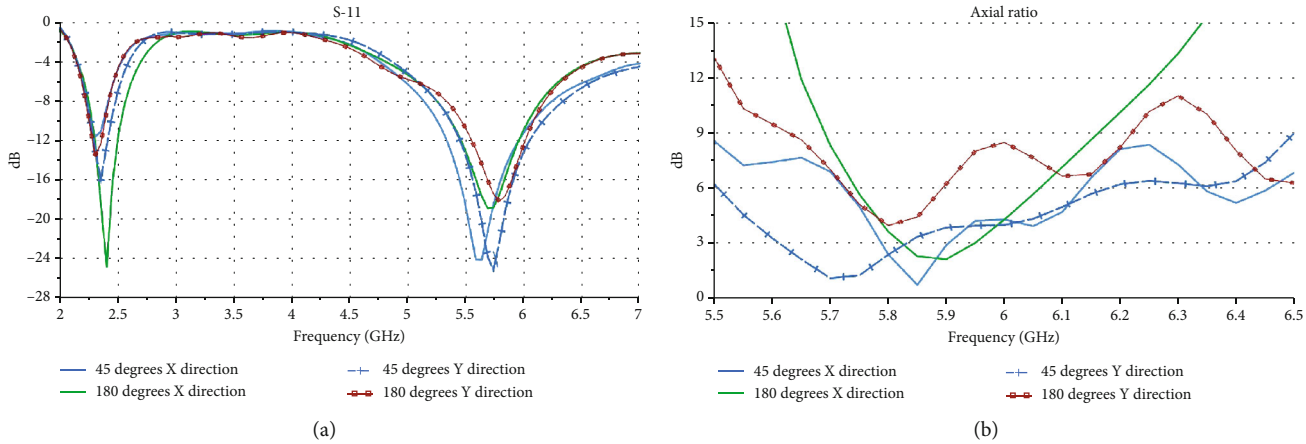

FIGURE 7: (a) S-11 parameter of the antenna in 45 and 180° bending conditions in *XZ* and *YZ* planes. (b) Axial ratio of the antenna in 45 and 180° bending conditions in *XZ* and *YZ* planes.

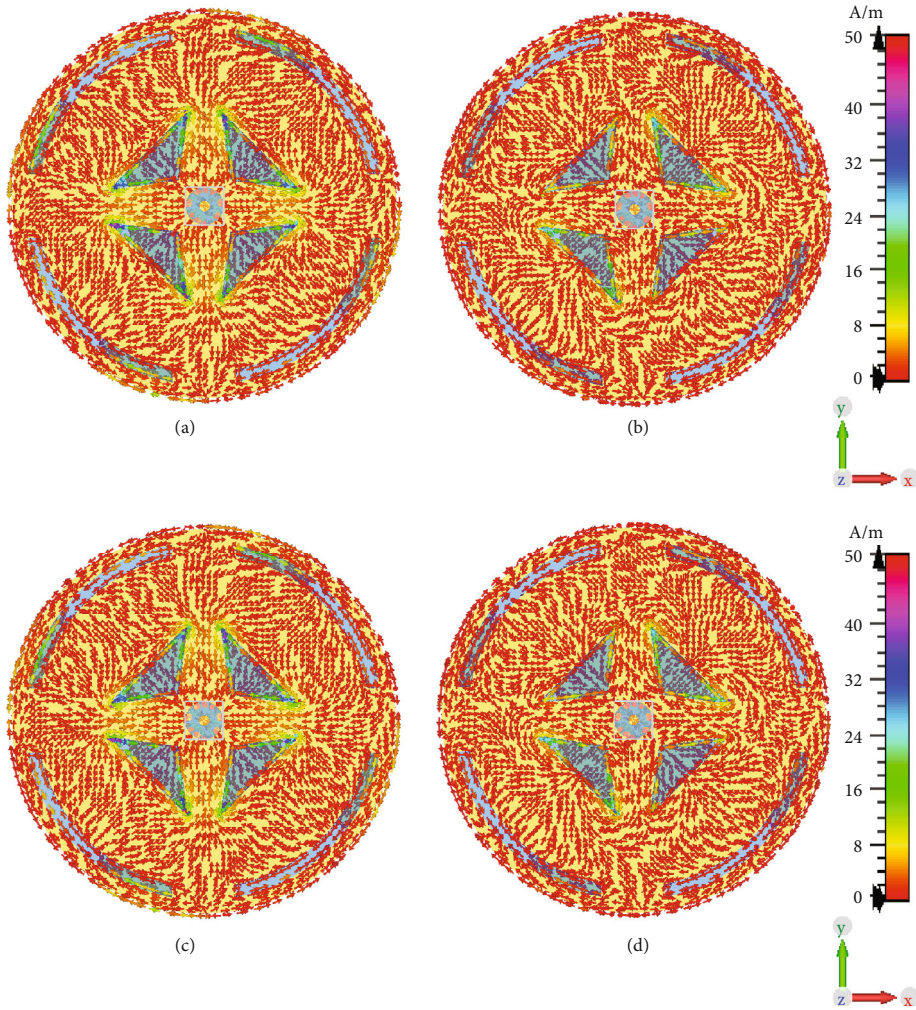

FIGURE 8: Surface current distribution of ground layer in 5.8 GHz. (a) Surface current distribution in phi = 0. (b) Surface current distribution in phi = 90. (c) Surface current distribution in phi = 180. (d) Surface current distribution in phi = 270.

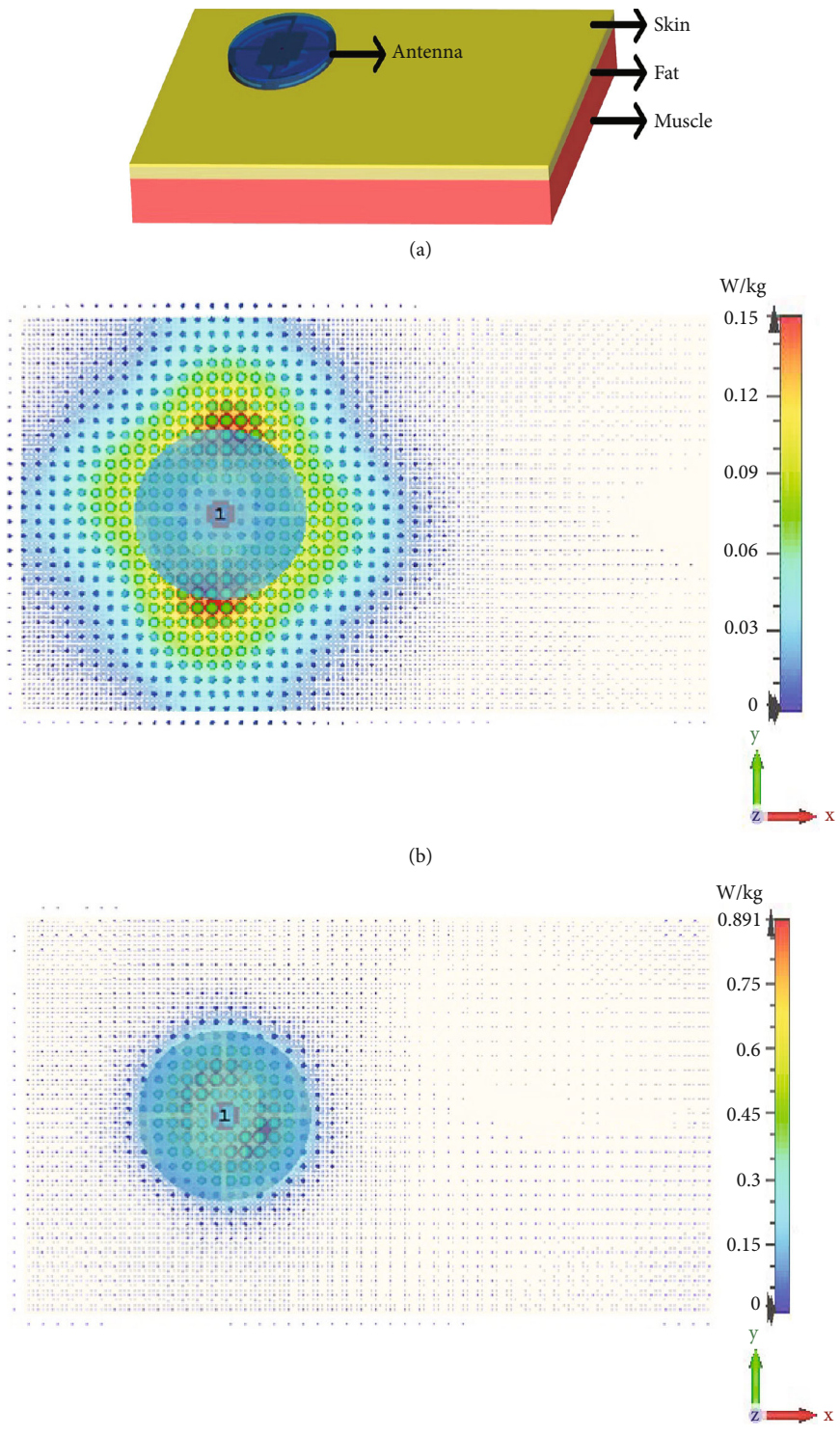

FIGURE 9: (a) Antenna on human body tissue. (b) Simulated SAR in 2.4 GHz. (c) Simulated SAR in 5.8 GHz.

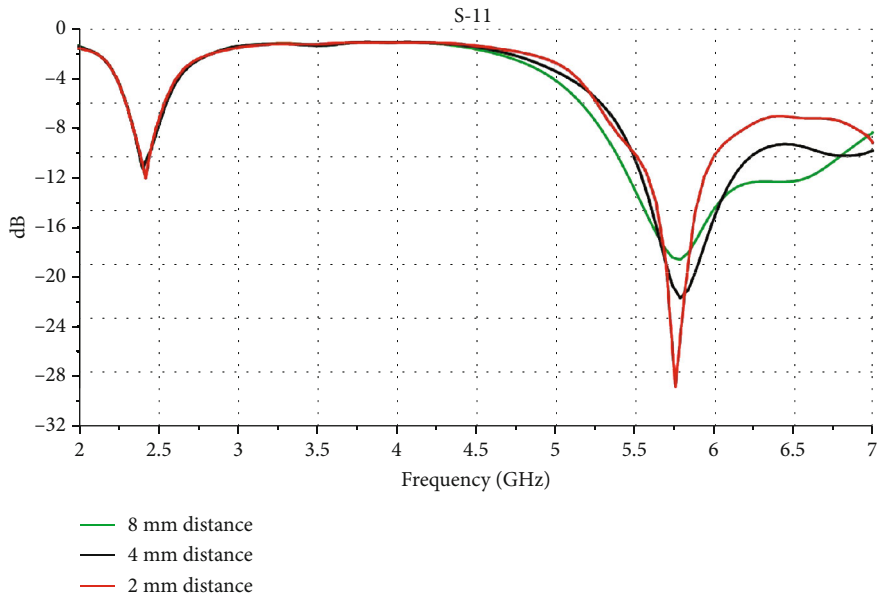

Figure 10: Simulated S-11 parameter of the antenna in different distances from the human body tissue.

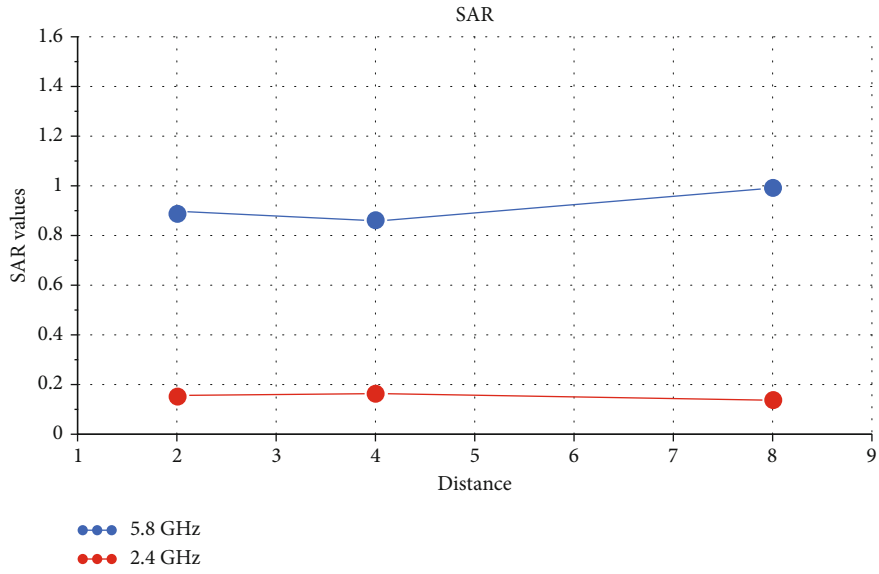

Figure 11: Simulated SAR vales at different distances from body tissue. Red dots are SAR values in 2.4 GHz, and blue dots are SAR values in 5.8 GHz.

properties of the phantom used in the simulation process which consists of skin, fat, and muscle layers are given in Table 2.

A graphic voxel human model is presented in Figure 12 with the antenna attached to the wrist and arm of the model to illustrate a visual utilization of on-body usage.

According to the IEEE standard of acceptable SAR values which is IEEE C95.1-2005 *IEEE Standard for Safety Levels With Respect to Human Exposure to Radio Frequency Electromagnetic Fields, 3 kHz to 300 GHz*, the actual simulated value for a 1 g average tissue should be less than 1.6 Wkg. Simulated antenna accords with the mentioned value when placed within the distance of having a cloth over the skin. The relative values are 0.152571 Wkg in 2.4 GHz and 0.891062 Wkg in 5.8 GHz. A proper distance should be chosen for implementing the antenna over the user's skin in order not to overheat the surface and the characteristics like gain and radiation pattern kept in a proper range similar to the antenna's performance in free space [22].

4. Fabrication and Measured Results

The antenna is designed in a way to maximize the simplicity of fabrication process. The measured height of each jean

Table 2: Electromagnetic properties of different human body tissues [21].

Body tissue	Conductivity (Sm)	Density $(kg(m^3))$	Permittivity
Skin	1.46 in 2.4 GHz–3.72 in 5.8 GHz	1100	38 in 2.4 GHz–35.1 in 5.8 GHz
Fat	0.1 in 2.4 GHz–0.29 in 5.8 GHz	916	5.3 in 2.4 GHz–5 in 5.8 GHz
Muscle	1.88 in 2.4 GHz–5.44 in 5.8 GHz	1041	54.4 in 2.4 GHz–49.5 in 5.8 GHz

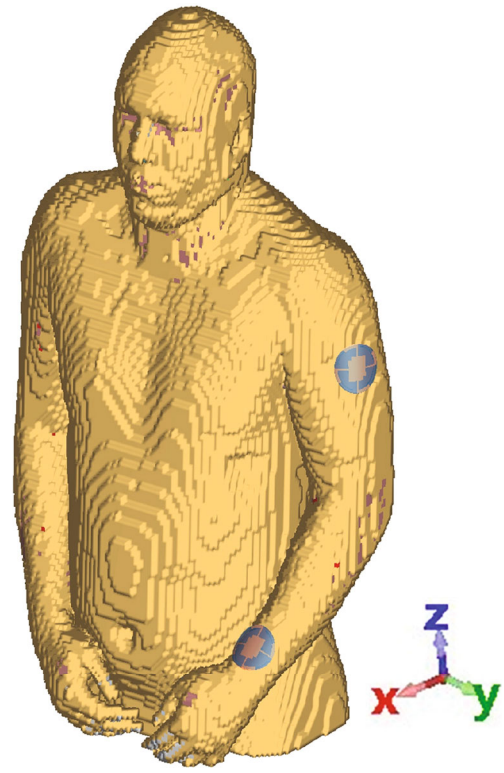

Figure 12: Antenna attached to the arm and wrist of the user.

fabric layer is approximately 0.7 mm. For substrate of the structure, three jean fabric layers are embroidered together to reach the predesigned height and to be in accordance with computer-based simulations. Thin copper layers used as patch and ground layers of the antenna are attached to three embroidered layers of jean fabric layers using adhesive glue to ensure the mitigation of changing the dielectric properties of the substrate of the antenna. A superstrate of one jean fabric layer is mounted on the patch layer. This superstrate layer not only enhances some of the radiation characteristics of the antenna but also provides a decent level of unity with user's clothing. An SMA connector is soldered symmetrically to the ground layer center in a way not to overlap with defects in antenna's ground in order not to deteriorate the designed ground layer properties caused by mentioned defects in it. The pin of the SMA connector is directly soldered to the center of the patch of the antenna. Figure 13 shows the fabricated antenna. As it was designed, the antenna is acceptably flexible and shows adequate accordance with the user's outfit whether it is attached to the user's sleeve or elsewhere. Simulated and measured *S* parameter is shown in Figure 14. As Figure 14 shows, the structure suffers from resonance frequency shifts in both lower and upper bands. To justify this deviation, the fabrication process should be taken into account. Unwanted trapped air between jean fabric layers of the substrate, which occurs due to simple assembly of the structure and deficiency of unity between three jean fabric layers, decreases the actual permittivity of the dielectric medium between patch and ground layers and consequently results in resonance frequency shifts. Measured *S* parameter of the antenna shows that the amount of return loss in 2.4 GHz is −17 dB which is quite acceptable for a planar structure. The bandwidth in this band is around 200 MHz (2.3–2.5 GHz) that is practically decent for indoor usages. In the upper band, return loss is dramatically ameliorated and reaches −28 dB and delivers 500 MHz of bandwidth.

The antenna is tested in the antenna measurement room, and the extracted radiation patterns are in acceptable harmony with simulated patterns. Simulated and measured CO polarization patterns are presented in the E plane in both frequencies, and the combined results are shown in

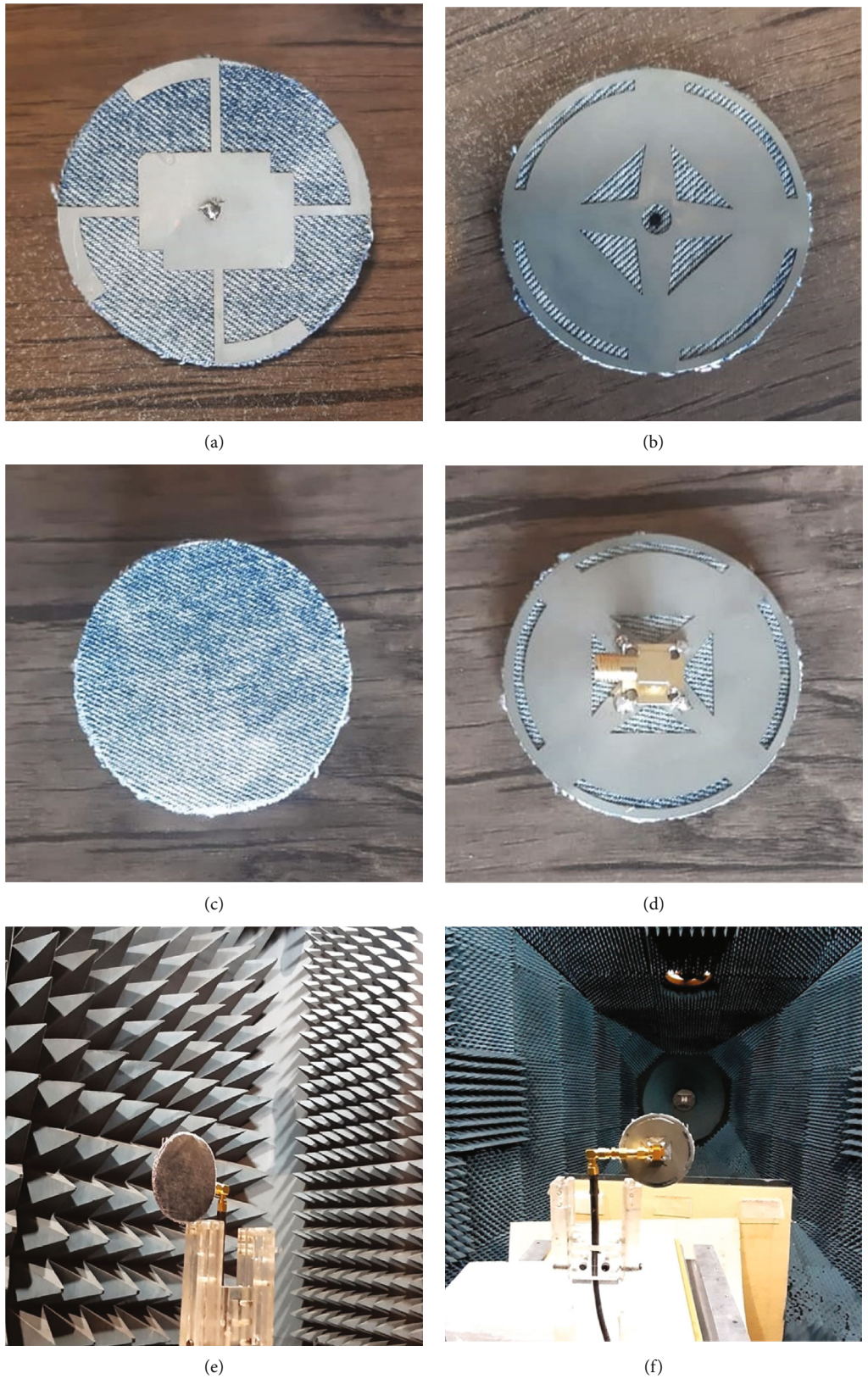

FIGURE 13: (a) Top view without superstrate. (b) Bottom view without SMA connector. (c) Top view with superstrate mounted on. (d) Bottom view with SMA connector soldered to the ground. (e) Front view in the anechoic chamber. (f) Back view in the anechoic chamber.

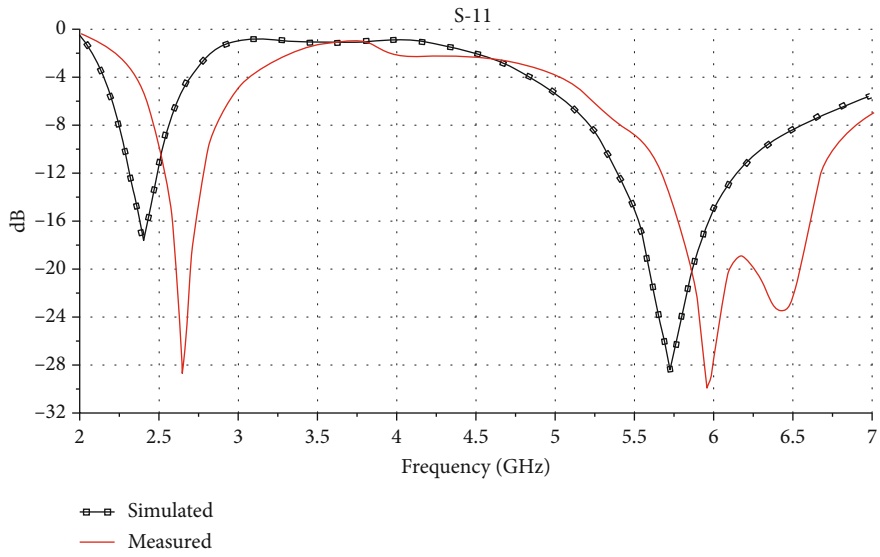

FIGURE 14: S-11 parameter of the proposed antenna. Black line depicts the simulated results, and red line depicts the measured results.

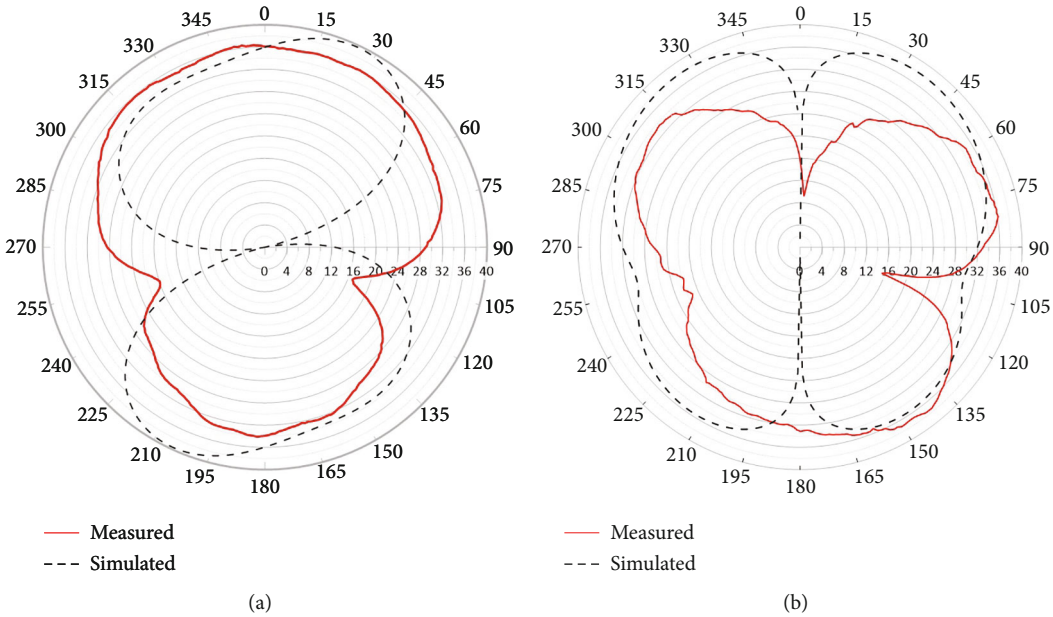

FIGURE 15: (a) CO polarization polar pattern in 2.4 GHz. (b) CO polarization polar pattern in 5.8 GHz. Black dashed line is the simulation pattern, and red line is the measured pattern.

the form of polar patterns in Figure 15. Achieving the radiation properties including measured radiation patterns of the proposed antenna shown in Figure 15 is done in the anechoic chamber with cylindrical antenna measurement setup. A horn antenna is used as the measurement antenna (MA) and the antenna under test (AUT) as the receiver with the distance of 6 m from each other. AUT is mounted on a turntable to gather the received angular data from the MA. Employing this method for two principal axes of the AUT provides achieving radiation parameters in both E and H planes.

As all the measured and simulated results demonstrate, on-body communication would be possible with other medical sensors which are attached to the patient's body due to the radiation pattern achieved in the lower working band. Off-body communication with farther devices in medical environments is provided by means of circular polarization which helps the wearer to easily move around with maximum rate of data transmitting and a more directional radiation pattern in the upper working band. A brief comparison between the proposed antenna and other references is presented in Table 3.

Table 3: Performance comparison between the proposed structure and other studies.

Reference	Dimensions (mm^3)	Frequency (GHz)	−10 dB BW (%)	Gain (dBi)	Polarization (AR BW (%))	Application
[3]	$50 \times 50 \times 2.76$	2.4	9	6.06	Circular (2.5)	On-body
[23]	$\pi \times 25^2 \times 5$	2.45/5.8	10/9	−5.1/3.3	Linear/circular (19)	On-body
[14]	$55 \times 55 \times 1.1$	2.45/5	4/16	3.9/5.2	Linear	On-body
[17]	$53 \times 34 \times 1.5$	5.4	3	2.9	Circular (not mentioned)	Not mentioned
[24]	$61.5 \times 61.5 \times 11$	2.45/5.8	8/25	5.67/6.89	Linear	On-body
[25]	$\pi \times 25^2 \times 4$	2.45/5	1.2/39.7	2.7/7	Linear	On-body
[26]	$\pi \times 27.52 \times 4$	5.45	12	7.6	Linear	On-body
[27]	$34 \times 30 \times 2$	2.4/5.1	6/3	1.45/1.55	Linear	On-body
[28]	$82 \times 74 \times 1$	2.44/5.8	4.8/9	3.8/2.15	Linear	On-body
[29]	$40 \times 50 \times 1.524$	5.8	86	8.2	Circular (23)	On-body
Proposed	$\pi \times 30^2 \times 3.3$	2.4/5.8	10/24	1.1/3.9	Linear/circular (4.2)	On/off-body

5. Conclusion

In this literature, a dual-band wearable antenna is proposed which features circular polarization in the upper working band and linear polarization in the lower transmission band. It is implemented on jean fabric layers as the dielectric material which provide flexibility for wearing and homogeneousness to the usual pieces of clothes. The parameters of this antenna are precisely calculated, and different parametric studies on conductor layers and bending situations are provided to guarantee the possibility of usage in the medical environment for healthcare monitoring and other interconnected medical purposes. To reduce any further complexity, one probe feeding port is used although dual polarization is achieved through coupling between the patch with four circular stubs and the DGS. SAR values have been calculated in both working bands by computer-based programs as a proof to show that the proposed structure is not harmful to the human body. The antenna is fabricated and tested in the anechoic chamber, and the results are adequately in accordance with the simulations.

Nomenclature

ISM industrial scientific medical
SAR specific absorption rate

Data Availability Statement

The data that support the findings of the study are available from the corresponding author upon reasonable request.

Conflicts of Interest

The authors declare no conflicts of interest.

Funding

The authors received no specific funding for this work.

References

[1] M. Mirmozafari, G. Zhang, C. Fulton, and R. J. Doviak, "Dual-polarization antennas with high isolation and polarization purity: a review and comparison of cross-coupling mechanisms," *IEEE Antennas and Propagation Magazine*, vol. 61, no. 1, pp. 50–63, 2019.

[2] M. Klemm and G. Troester, "Textile UWB antennas for wireless body area networks," *IEEE Transactions on Antennas and Propagation*, vol. 54, no. 11, pp. 3192–3197, 2006.

[3] C. Hertleer, H. Rogier, L. Vallozzi, and L. Van Langenhove, "A textile antenna for off-body communication integrated into protective clothing for firefighters," *IEEE Transactions on Antennas and Propagation*, vol. 57, no. 4, pp. 919–925, 2009.

[4] M. Allayioti, J. R. Kelly, and R. Mittra, "Beam and polarization reconfigurable microstrip antenna based on parasitics," *Microwave and Optical Technology Letters*, vol. 60, no. 6, pp. 1460–1464, 2018.

[5] C. Wu, C. Lu, and W. Cao, "Wideband dual-polarization slot antenna with high isolation by using microstrip line balun feed," *IEEE Antennas and Wireless Propagation Letters*, vol. 16, pp. 1759–1762, 2017.

[6] H. Lee, D. Ren, and J. H. Choi, "Dual-band and polarization-flexible CRLH substrate-integrated waveguide resonant antenna," *IEEE Antennas and Wireless Propagation Letters*, vol. 17, no. 8, pp. 1469–1472, 2018.

[7] T. Oh, Y. G. Lim, C. B. Chae, and Y. Lee, "Dual-polarization slot antenna with high cross-polarization discrimination for indoor small-cell MIMO systems," *IEEE Antennas and Wireless Propagation Letters*, vol. 14, pp. 374–377, 2015.

[8] A. Venouil, M. Egels, M. Benwadih, C. Serbutoviez, and P. Pannier, "Design guidance of a circularly polarized bowtie antenna for ISM bands," *Microwave and Optical Technology Letters*, vol. 65, no. 11, pp. 2972–2978, 2023.

[9] R. Salvado, C. Loss, R. Gonçalves, and P. Pinho, "Textile materials for the design of wearable antennas: a survey," *Sensors*, vol. 12, no. 11, pp. 15841–15857, 2012.

[10] K. N. Paracha, S. K. A. Rahim, P. J. Soh et al., "A low profile, dualband, dual polarized antenna for indoor/outdoor wearable application," *IEEE Access*, vol. 7, pp. 33277–33288, 2019.

[11] J. M. Felício, J. R. Costa, and C. A. Fernandes, "Dual-band skin-adhesive repeater antenna for continuous body signals monitoring," *IEEE Journal of Electromagnetics, RF and Microwaves in Medicine and Biology*, vol. 2, no. 1, pp. 25–32, 2018.

[12] S. Mener, R. Gillard, and L. Roy, "A dual-band dual-circular-polarization antenna for Ka-band satellite communications," *IEEE Antennas and Wireless Propagation Letters*, vol. 16, pp. 274–277, 2017.

[13] I. Locher, M. Klemm, T. Kirstein, and G. Troster, "Design and characterization of purely textile patch antennas," *IEEE Transactions on Advanced Packaging*, vol. 29, no. 4, pp. 777–788, 2006.

[14] S. Zhu and R. Langley, "Dual-band wearable textile antenna on an EBG substrate," *IEEE Transactions on Antennas and Propagation*, vol. 57, no. 4, pp. 926–935, 2009.

[15] M. L. Scarpello, I. Kazani, C. Hertleer, H. Rogier, and G. D. Vande, "Stability and efficiency of screen-printed wearable and washable antennas," *IEEE Antennas and Wireless Propagation Letters*, vol. 11, pp. 838–841, 2012.

[16] S. Sankaralingam and B. Gupta, "Determination of dielectric constant of fabric materials and their use as substrates for design and development of antennas for wearable applications," *IEEE Transactions on Instrumentation and Measurement*, vol. 59, no. 12, pp. 3122–3130, 2010.

[17] M. Moubadir, I. Badaoui, N. A. Touhami, M. Aghoutane, and M. E. Ouahabi, "A new circular polarization dual feed microstrip square patch antenna using branch coupler feeds for WLAN/HIPERLAN applications," *Procedia Manufacturing*, vol. 32, pp. 702–709, 2019.

[18] D. Bhargava, N. Leeprechanon, P. Rattanadecho, and T. Wessapan, "Specific absorption rate and temperature elevation in the human head due to overexposure to mobile phone radiation with different usage patterns," *International Journal of Heat and Mass Transfer*, vol. 130, pp. 1178–1188, 2019.

[19] M. C. Gosselin, G. Vermeeren, S. Kuhn et al., "Estimation formulas for the specific absorption rate in humans exposed to base-station antennas," *IEEE Transactions on Electromagnetic Compatibility*, vol. 53, no. 4, pp. 909–922, 2011.

[20] A. Sabbah, N. Dib, and M. Al-Nimr, "Evaluation of specific absorption rate and temperature elevation in a multi-layered human head model exposed to radio frequency radiation using the finite-difference time domain method," *Microwaves, Antennas and Propagation, IET*, vol. 5, no. 9, pp. 1073–1080, 2011.

[21] A. Christ, T. Samaras, A. Klingenböck, and N. Kuster, "Characterization of the electromagnetic near-field absorption in layered biological tissue in the frequency range from 30 MHz to 6000 MHz," *Physics in Medicine and Biology*, vol. 51, no. 19, pp. 4951–4965, 2006.

[22] M. M. U. Rashid, L. C. Paul, A. Bouazizi, R. Sen, B. Podder, and A. K. Sarkar, "Effect of human body on an 800 MHz inset fed rectangular microstrip patch antenna characteristics," in *2017 International Conference on Electrical, Computer and Communication Engineering (ECCE)*, pp. 738–742, Cox's Bazar, Bangladesh, 2017.

[23] S. Bhattacharjee, S. Maity, S. R. B. Chaudhuri, and M. Mitra, "A compact dual-band dual-polarized omnidirectional antenna for on-body applications," *IEEE Transactions on Antennas and Propagation*, vol. 67, no. 8, pp. 5044–5053, 2019.

[24] S. Wang and H. Gao, "A dual-band wearable conformal antenna based on artificial magnetic conductor," *International Journal of Antennas and Propagation*, vol. 2022, no. 1, Article ID 9970477, 2022.

[25] R. Liu, J. W. Zhang, W. Q. Chen, Y. F. Zhang, Z. L. Mei, and T. M. Niu, "Design and verification of a dual-band wearable antenna based on characteristic mode theory," *IET Microwaves, Antennas & Propagation*, vol. 17, no. 7, pp. 536–546, 2023.

[26] G. Gao, R. F. Zhang, W. F. Geng, H. J. Meng, and B. Hu, "Characteristic mode analysis of a nonuniform metasurface antenna for wearable applications," *IEEE Antennas and Wireless Propagation Letters*, vol. 19, no. 8, pp. 1355–1359, 2020.

[27] T. H. Dam, M. T. Le, Q. C. Nguyen, and T. T. Nguyen, "Dual-band metamaterial-based EBG antenna for wearable wireless devices," *International Journal of RF and Microwave Computer-Aided Engineering*, vol. 2023, no. 1, Article ID 2232674, 2023.

[28] W. Thaiwirot, Y. Hengroemyat, T. Kaewthai, P. Akkaraekthalin, and S. Chalermwisutkul, "A dual-band low SAR microstrip patch antenna with jean substrate for WBAN applications," *International Journal of RF and Microwave Computer-Aided Engineering*, vol. 2024, no. 1, Article ID 5076232, 2024.

[29] M. N. Yende, G. Singh, G. A. Eyebe, C. Mbinack, and J. M. Mbida, "Implanted rhombus ring partial inset-fed circularly polarized microstrip monopole antenna for WBAN applications," *International Journal of RF and Microwave Computer-Aided Engineering*, vol. 2024, no. 1, Article ID 2555206, 2024.